Phase Transition in Two-dimensional Bose gas

Wenchao Xu

May 10, 2012

Department of Physics, University of Illinois at Urbana-Champaign, Urbana, IL, 61801

Abstract

Dimensionality of system plays a vital role in physics. Recent developments in ultracold gases provide the possibilities to explore low-dimensional region. In this paper, I will focus on two kinds of phase transitions in two-dimensional Bose gases: one is the Berezinskii-Kosterlitz-Thouless (BKT) phase transition; whose disordered state is characterized by the proliferation of topological vortices pairs; the other is the normal-to-superfluid transition occurred in optical lattice at the zero-temperature limit, the physics of which can be described by Bose-Hubbard Model. I will present theoretical approach to these two problems, and then discuss recent experimental results which provide a clear demonstration for these critical phenomena.

1 Introduction

Dimensionality plays a vital role in physics. A wealth of new phenomena associated with lower dimensions have been investigated both experimentally and theoretically, such as Dirac cone on graphene, quantum Hall effect and so on. Phase transition, one of the most fascinating phenomena in physics, is highly dimensional dependent. Taking the well-known Ising model as an example, if $d = 1$, there will be no phase transition at any finite temperature, but not the case if $d \geq 2$. Further study demonstrates that the critical exponents derived from mean field theory are not correct unless $d > 4$.

In conventional condensed matter physics, thin films or nanowires can be regarded as typical two- or one-dimensional system. While for cold atomic system, the ability to impose strong confinement along one direction in a trapping potential makes it possible to create highly flattened clouds of atoms, providing a well-controlled platform to study this area.

In this paper, I will focus on two interesting phenomena in two-dimensional Bose gas: one is Berezinskii-Kosterlitz-Thouless (BKT) transition, which is special since the system goes from disorder to quasi-long-range order state; the other is quantum phase transition described by Bose Hubbard model occurred in the vicinity of zero temperature. Optical lattice formed by standing waves provides an ideal emulator of this model.

2 Berezinskii-Kosterlitz-Thouless (BKT) Transition

BKT transition is an important phase transition occurred at two-dimensional system. It involves the emergence of topological charge pairs (i.e. vortices) above a critical temperature. By the fact that in thermal equilibrium at finite temperature, the free energy $F = E - TS$ must be minimized, it is easy to capture the physical picture of BKT transition. Because the excitation energy corresponding to a vortex is $\frac{\rho_s}{2}\int_a^L d^2r\frac{1}{r^2} = \pi\rho\ln\frac{L}{a}$, while the number of possible configurations to create a vortex in the system with area L^2 is $\frac{L^2}{a^2}$, the change in free energy $\Delta F = \pi\rho_s\ln\frac{L}{a} - 2T\ln\frac{L}{a}$. If $T > T_c = \frac{\pi\rho_s}{2}$, the proliferation of vortices is preferable.

2.1 XY Model[1]

As a theoretical preparation for our following discussion, the classical XY model is introduced first. As we will see later, it can describe BKT transition. The Hamiltonian of a classical XY model on a two-dimensional orthogonal lattice sites is

$$H_{XY} = -J\sum_{<i,j>} cos(\theta_i - \theta_j), \tag{1}$$

where $\langle i, j\rangle$ indicates nearest-neighbour sites. By expanding it to quadratic term, we have

$$cos(\theta_i - \theta_j) \approx 1 - \frac{1}{2}(\theta_i - \theta_j)^2.$$

The validity of the above approximation requires $\theta_i - \theta_j$ is small compared with π. To fulfill it, we can write $\theta_i - \theta_j = 2\pi n + \epsilon$ ($\epsilon \ll \pi$), then the partition function becomes

$$Z = e^{-\beta H_{XY}} = \exp[\beta J\sum_{\langle i,j\rangle} cos(\theta_i - \theta_j)] \rightarrow \sum_{m=-\infty}^{\infty} e^{\beta J}\exp\{\sum_{\langle i,j\rangle}[-\frac{\beta J}{2}(\theta_i - \theta_j - 2\pi m)^2]\}.$$

For the right-hand side, the term with minimum value of $(\theta_i - \theta_j - 2\pi m)^2$ dominates, and this term supports the above approximation.

To transform the above expression into a Gaussian integral, we use Poisson's equation,

$$\sum_{m=-\infty}^{\infty} h(m) = \sum_{l=-\infty}^{\infty} \int_{-\infty}^{+\infty} d\phi h(\phi) e^{2\pi i l \phi},$$

and up to some constant factor, the partition function becomes

$$\begin{aligned} Z = \sum_{m=-\infty}^{\infty} e^{\beta J} e^{\sum_{\langle i,j \rangle} [-\frac{\beta J}{2}(\theta_i - \theta_j - 2\pi m)^2]} &\sim \int D\theta \sum_{l_{ij}=-\infty}^{\infty} \int d\phi e^{\beta J} e^{\sum_{\langle i,j \rangle} [-\frac{\beta J}{2}(\theta_i - \theta_j - 2\pi\phi)^2 + 2\pi i l_{ij}\phi]} \\ &= \int D\theta \sum_{\{l_{ij}\}} \exp\{-\sum_{<i,j>} [\frac{l_{ij}^2}{2\beta J} - i l_{ij}(\theta_i - \theta_j)]\} \end{aligned}$$

Since $l_{i,j}$ is defined for each pair of $\langle i, j \rangle$, we could rewrite it as a vector potential $l_u(r)$, $(u = (x, y))$, while r starts from the original point to the left or lower point in $\langle i, j \rangle$. Then the exponent term becomes

$$-\sum_{r,u} [\frac{l_u(r)^2}{2\beta J} - i l_u(r) \cdot (\theta(r) - \theta(r+u)]$$

Rewriting the second term $l_u(r) \cdot (\theta(r) - \theta(r+u)$ as $(l_u(r) - l_u(r-u)) \cdot \theta(r)$ makes it easy to perform integral over θ. We obtain

$$Z = \sum_{\{l_u(r)\}} \exp(-\sum_{r,u} \frac{l_u(r)^2}{2\beta J}) \prod_r \delta_{\sum_u (l_u(r) - l_u(r-u)),0}$$

The constraint imposed by the delta function is

$$\sum_u (l_u(r) - l_u(r-u)) = 0,$$

which is nothing but the discrete version of $\nabla \vec{l} = 0$. That is to say, we can find a vector field $\vec{n}(r)$ satisfying $\vec{l}(r) = \nabla \times \vec{n}(r)$, where $\vec{n}(r) = \vec{e}_z n(r)$. In the discrete version, $\nabla \times \vec{n}(r) = (\partial_y n(r), -\partial_x n(r)) = (n(r) - n(r-y), -n(r) + n(r-x))$, therefore, $l_u(r)^2 = (n(r) - n(r-u))^2$. The partition function becomes

$$Z = \sum_{\{n(r)\}} \exp[-\frac{1}{2\beta J} \sum_{r,\mu} (n(r) - n(r-u))^2]$$

Using Poisson's equation again, we have

$$Z = \int_{-\infty}^{\infty} D\phi \sum_{m=-\infty}^{\infty} \exp[-\frac{1}{2\beta J} \sum_{r,\mu} (n(r) - n(r-u))^2 + 2\pi i \sum_r m(r)\phi(r)].$$

By Fourier transformation to momentum space, we have

$$\begin{aligned} Z &= \int_{-\infty}^{\infty} D\phi \sum_{m=-\infty}^{\infty} \exp\{-\frac{1}{2\beta J}\int dk\phi_k[\sum_{\mu}(2-e^{ik\mu}-e^{-ik\mu})]\phi_k + 2\pi m(-k)\phi(k)\} \\ &= Z_{s.w}\sum_{m(r)=-\infty}^{\infty} exp[2\pi^2\beta J\sum_{r,r'} m(r)C(r-r')m(r')], \end{aligned} \tag{2}$$

where $C(r-r') = -\int \frac{dk_x}{2\pi}\int \frac{dk_y}{2\pi}\frac{e^{ik(r-r)}}{4-2\cos k_x - 2\cos k_y} \to \frac{1}{2\pi}\ln(\frac{|r-r'|}{a}) + \frac{1}{4} - G(0)$ for large $|r-r'|$. The term with $G(0)$ is $G(0)[\sum_r m(r)]^2$. If we interpret $m(r)$ as a "charge", this term will vanish due to the neutrality condition. The contribution from the constant also vanishes.

$Z_{s.w}$ is the contribution from spin wave part. It corresponds to the case where the fluctuations between i and j are suppressed, i.e. $m = 0$. As a function of ϕ, it is hard to transform $Z_{s.w}$ back to the presentation of θ. However, we could see easily that if $\theta_i - \theta_j$ is small, Eqn.(1) could be approximated as $\frac{J}{2}\int d^2r(\nabla\theta)^2$, so $Z_{s.w} = \exp[-\frac{J\beta}{2}\int d^2r(\nabla\theta)^2]$.

2.2 XY Model and BKT transition

In this section, we will build up the bridge between XY model and a two-dimensional superfluid system. In the absence of vorticity, the velocity of this flow can be written as $\vec{v_0} = \nabla\Phi$. The existence of vortex can be related to the vorticity $\nabla \times \vec{v}$. Notice that for any closed path, $\oint d\vec{l}\cdot\vec{v} = \int d^2r\nabla\times\vec{v}\cdot\vec{e_z} = 2\pi n$, ($n$ is an integer that reflects the total topological charges within that area.) One can set $\nabla\times\vec{v} = 2\pi\vec{e_z}\sum_i n_i\delta(r-r_i)$, describing a collection of vortices with topological charge $\{n_i\}$ at locations $\{r_i\}$.

By setting $\vec{v} = \vec{v_0} - \nabla\times(\vec{e_z}\psi)$, we have

$$\nabla\times\vec{v} = \vec{e_z}\nabla^2\psi \Rightarrow \nabla^2\psi = 2\pi\sum n_i\delta(r-r_i).$$

The field ψ just behaves like a potential created by a set of point charges and the solution for $d = 2$ is $\psi(r) = \sum_i n_i\ln(|r-r_i|) = 2\pi\sum_i n_i C(|r-r_i|)$.

The action of this system can be written as

$$\begin{aligned} S &= \frac{\beta}{2}\int d^2r\rho_s\vec{v}^2 = \beta\frac{\rho_s}{2}\int d^2r[\vec{v_0} - \nabla\times(\vec{e_z}\psi)]^2 \\ &= \frac{\rho_s\beta}{2}\int d^2r[(\nabla\Phi)^2 - 2\nabla\phi\cdot\nabla\times(\vec{e_z}\psi) + (\nabla\times(\vec{e_z}\psi))^2]. \end{aligned}$$

An integration by parts shows that the second term vanishes, while the third term

$$\begin{aligned} \int d^2r(\nabla\times(\vec{e_z}\psi))^2 &= \int d^2r(\partial_y\psi, -\partial_x\psi)\cdot(\partial_y\psi, -\partial_x\psi) = \int d^2r[(\partial_y\psi)^2 + (-\partial_x\psi)^2] \\ &= -\int d^2r\psi\nabla^2\psi = -4\pi^2\sum_{ij} n_i n_j C(|r_i - r_j|) \end{aligned}$$

The final expression for the action is

$$S = \frac{\rho_s\beta}{2}\int d^2r(\nabla\Phi)^2 - 2\pi^2\rho_s\beta\sum_{ij} n_i n_j C(|r_i - r_j|) \equiv S_{s.w} + S_t,$$

which matches Eqn.(2) in previous section. It is clear that $m(r)$ and J there represent the topological charge and superfluid density ρ_s, respectively. Moreover, the unphysical divergence at $i = j$ can be regularized by the core energy of a vortex, hence $S_t = \sum_i S_i^{core} - 4\pi^2 J \sum_{i<j} C(|r_i - r_j|)$.

2.3 Renormalization Group Approach

As we have seen, the partition function can be separated into two parts. In following discussion, we will focus on the topological part, with only elementary excitations (i.e. $n_i = \pm 1$). Notice that the system behaves just like Coulomb gas in 2D, so the effect of screening must be taken into consideration. To lowest order, the effective interaction between r and r' can be approximated by involving only two external "charges" (positioned at s and s'); it becomes

$$\begin{aligned}
\left\langle e^{-4\pi^2 \tilde{J} C(r-r')} \right\rangle &\simeq \frac{e^{-4\pi^2 \tilde{J} C(r-r')} + y_0^2 \int d^2s d^2s' e^{-4\pi^2 \tilde{J} C(s-s') - 4\pi^2 \tilde{J} C(r-r') + 4\pi^2 \tilde{J}[C(r-s)+C(r'-s')-C(r'-s)-C(r-s')]}}{1 + y_0^2 \int d^2s d^2s' e^{-4\pi^2 \tilde{J} C(r-r')}} \\
&\simeq e^{-4\pi^2 \tilde{J} C(r-r')} [1 + 16\pi^5 \tilde{J}^2 y_0^2 C(r-r') \int dx x^3 e^{-2\pi \tilde{J} ln(x)}] \\
&\simeq e^{-4\pi^2 \tilde{J} C(r-r')[1 - 4\pi^3 \tilde{J}^2 y_0^2 \int dx x^{3-2\pi\tilde{J}}]},
\end{aligned}$$

where $\tilde{J} = J/k_B T$ and $y_0 = e^{-S_{\pm 1}^{core}}$. Then we obtain $S_{eff}(r-r') = 4\pi^2 \tilde{J}_{eff} C(r-r')$, where

$$\tilde{J}_{eff} = \tilde{J} - 4\pi^3 \tilde{J}^2 y_0^2 \int dx x^{3-2\pi\tilde{J}}$$

The renormalization procedure is conducted by breaking this integral into two parts: $\int_a^\infty = \int_a^{e^l a} + \int_{e^l a}^\infty$. The non-singular short-distance contribution can be evaluated and incorporated into $\tilde{J}$. The remaining integral can be rescaled by $e^l a \to a$ and reach the differential recursion relations[2]:

$$\begin{aligned}
\frac{d\tilde{J}^{-1}}{dl} &= 4\pi^3 a^4 y_0^2 + O(y_0^4) \\
\frac{dy_0}{dl} &= (2 - \pi L) y_0 + O(y_0^3)
\end{aligned}$$

The renormalization flows are shown in Fig.(1). With $\tilde{J}^{-1} \leq \frac{\pi}{2}$, the low-temperature phase is characterized by a line of fixed points where $y_0 \to 0$. It indicates that there is no unbound vortices in this case. Here the correlation length decays as a power law, the suppression of fluctuations leads to $\langle cos(\theta(r) - \theta(0)) \rangle \simeq e^{-\frac{1}{2}\left\langle (\theta(r)-\theta(0))^2 \right\rangle} = (\frac{a}{r})^{1/2\pi J*} \sim r^{-\eta}$, with $\eta = \frac{1}{2\pi J*} \leq 1/4$, indicating a quasi-long-range order. In the high-temperature phase, $y_0 \to \infty$ and $J \to 0$, free vortices' pairs emerge. Correlation length decays exponentially:

$$\begin{aligned}
\langle \cos(\theta(r) - \theta(0)) \rangle &= \frac{1}{Z} \prod_{i=1}^N (\int_0^{2\pi} \frac{d\theta_i}{2\pi}) \cos(\theta(r) - \theta(0)) e^{\tilde{J} \sum_{i,j} cos(\theta_i - \theta_j)} \\
&\simeq \frac{1}{Z} \prod_{i=1}^N (\int_0^{2\pi} \frac{d\theta_i}{2\pi}) \cos(\theta(r) - \theta(0)) \prod_{i,j} [1 + \tilde{J} \sum_{i,j} cos(\theta_i - \theta_j)] \\
&\sim (\frac{J}{2})^r \sim exp[-\frac{r}{\xi}],
\end{aligned}$$

where the correlation length $\xi^{-1} \equiv \ln(2/J)$. ξ goes to zero under RG flow.

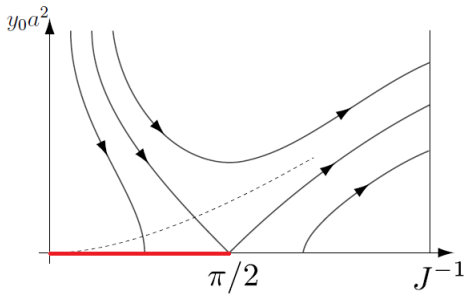

Figure 1: Schematic of RG flow. The red curve indicates the line of fixed points below T_c.

2.4 Experimental Study on BKT Transition

In this section, BKT transition observed in cold bosonic atoms are discussed[3]. As shown in Fig.2(a), two copies of 2D atomic cloud are prepared at the nodes of 1D optical lattice potential. After the trapped 2D gases reach equilibrium, they are released. A camera records the information about the matter wave interference between them (Fig.2(b)). The vertical fringes are due to the interference of these two copies, while the waviness of the interference fringes contains the information about the phase patterns in each planar system.

The temperature of the system is determined from the central contrast of the interference pattern, which quantifies the degeneracy of the 2D system and so the temperature. Higher c_0 reflects lower temperature. Integrate the interference pattern along x and the resulting contrast c will decay with the integration length. The average value of c^2 should behave as[4]

$$\left\langle c^2(L_x)\right\rangle \approx \frac{1}{L_x}\int_0^{Lx} dx[C(x,0)]^2 \propto (\frac{1}{L_x})^{2\alpha}$$

Above critical temperature T_c, assuming correlation function $C(x,0)$ decays exponentially on a length scale much shorter than L_x, the integral should be independent of L_x, i.e $\langle c^2(L_x)\rangle \sim \frac{1}{L_x}$, so $\alpha = 0.5$. Conversely, just below T_c, $C \propto x^{-\frac{1}{4}}$ as shown in section 2.3, so α equals to 0.25. Fig.2(c) demonstrates the change of α from 0.5 to 0.25 versus decreasing temperature. Due to the finite size effect, the transition occurs as a finite-width crossover rather than a sharp phase transition. Fig.2(d) proves the proliferation of free vortices at higher temperature. The dislocations in the interference image is interpreted as vorteices, whose number enhances with increasing temperature.

3 Quantum Criticality

Unlike thermally induced phase transition, quantum phase transition can take place at zero temperature, driven by external parameters. Generally speaking, for arbitrary Hamiltonian, its kinetic part H_0 and potential part V do not commute and therefore $e^{-\beta H} \neq e^{-\beta H_0}e^{-\beta V}$, but for finite β, we could have $e^{-\beta H} = [e^{-\delta\tau(H_0+V)}]^N \approx [e^{-\delta\tau H_0}e^{-\delta\tau V}]^N$ where $\delta\tau = \beta/N$. However, at zero-temperature, $\beta \to \infty$, the static and dynamic part are inextricably linked and impossible to separate. Consequently, the d-dimensional quantum system behaves like a d+1-dimensional classical system, with an extra degree of freedom comes from dynamics.

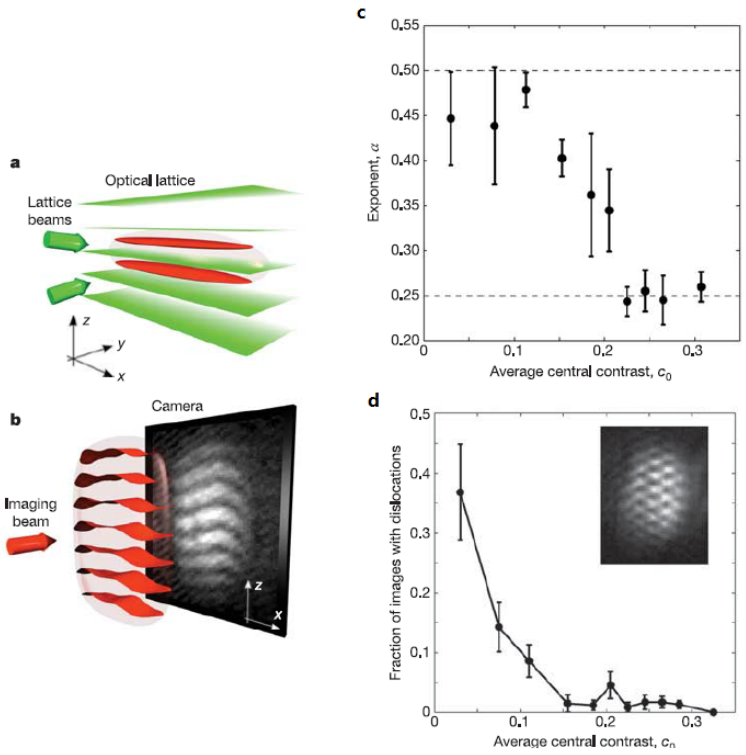

Figure 2: Schematic of (a) the experimental preparation of 2D cloud of bosons and (b) imaging system. After releasing from trap, the two clouds expand predominantly along z-axis and overlap to form a interference patten. The camera records the pattern at x-z plane. (c) Emergence of quasi-long-range order in a 2D gas. Dashed lines indicate the theoretical expected values of α above and just below T_c. Higher c_0 corresponds to lower temperature. (d) Proliferation of free vortices with increasing temperature. The sharp dislocations in the inset are attributed to the presence of a free vortex. The figure shows the number of vortices as a function of c_0.

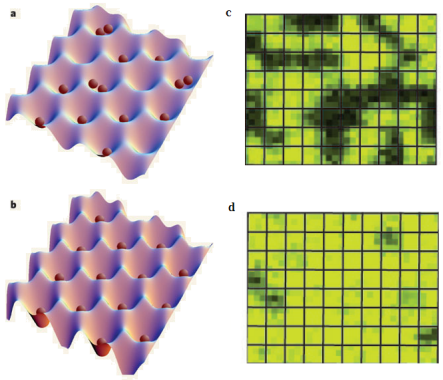

Figure 3: Schematic of (a) superfluid and (b) Mott insulator in an optical lattice. (c) and (d) are experimental single-site fluorescence imaging of atom number for superfluid and Mott insulator. The bright dot means the site is occupied by one atom, while black dot indicates that the site is either empty or occupied by two atoms. (From Ref[5])

3.1 Introduction to Bose-Hubbard Model

The Hamiltonian of Bose-Hubbard model is

$$H_{BH} = -J \sum_{<i,j>} \hat{b}_i^\dagger \hat{b}_j + \sum_i (\varepsilon_i - \mu)\hat{n}_i + \sum_i \frac{1}{2} U \hat{n}_i(\hat{n}_i - 1),$$

where J is the hopping coefficient that describes the tunneling of bosons between nearest neighbour sites, U describes the on-site repulsive interaction between two particles, and $\hat{n}_i = \hat{b}_i^\dagger \hat{b}_i$ counts the number of bosons on i^{th} lattice site. For a homogenous system, ε_i is a constant and therefore can be absorbed into the chemical potential μ.

Before doing any analytical calculation, we could consider two limit cases first. (1): $U/J \gg 1$. In this case, each site should be occupied by an integer number which minimize

$$\varepsilon(n) = -\mu n + \frac{1}{2} U n(n-1),$$

whose result shows that for $n - 1 < \mu/U < n$, exactly n bosons will occupy each site. The system is in Mott insulator state. (2): $J/U \gg 1$. The kinetic term dominates; atoms are delocalized. It is superfluid and the ground state can be described by a macroscopic wavefunction. The cartoons and real experimental images for these two phases are shown in Fig.3.

To perform quantitative analysis, the partition function is represented by coherent path integral in imaginary time:

$$Z = \int D b_i D b_i^\dagger \exp\{-\int_0^\beta d\tau [\sum_i b_i^\dagger (\partial_\tau - u) b_i + \frac{U}{2} b_i^\dagger b_i^\dagger b_i b_i - \sum_{i,j} J_{i,j}(b_i^\dagger b_j + b_j^\dagger b_i)]\}. \quad (3)$$

As a first step, we decouple the non-local hopping term by performing Hubbard-Stratanovich transformation,

$$\exp[\int_0^\beta d\tau \sum_{i,j} J_{i,j} b_i^\dagger b_j] = \int D\psi \exp\{-\int_0^\beta d\tau [\sum_{i,j} \psi_i^* J_{i,j}^{-1} \psi_j - \sum_{<i,j>} (b_i^\dagger \psi_j + \psi_i^* b_j)]\},$$

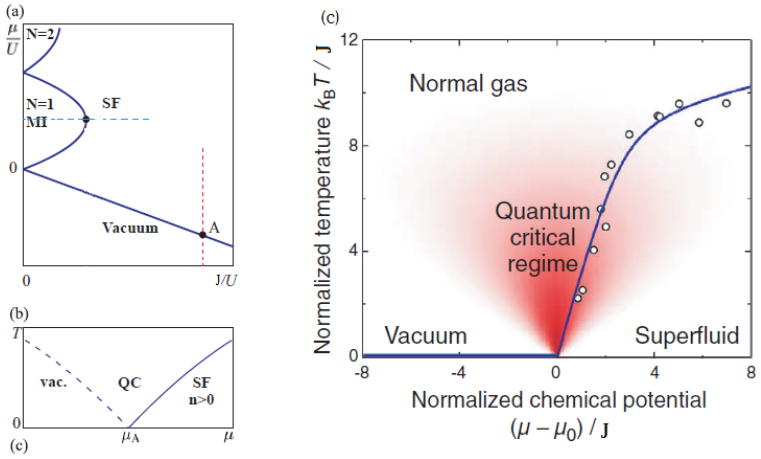

Figure 4: (a) The phase diagram of Bose Hubbard model at $T = 0$. (b) Finite-temperature phase diagram along the red line and (c) corresponding experimental data. ((a),(b) from Ref.[7], (c) from Ref.[8])

the partition function becomes

$$Z = \int D\psi \exp\{\int d\tau \sum_{ij} -J_{ij}^{-1}\psi_i^*\psi_j + \log\left\langle \exp[\int d\tau \sum_{i,j}(b_i^\dagger\psi_j + \psi_i^* b_j)]\right\rangle_{S_{loc}}\}$$

where $< ... >_{loc} = \int ...e^{-\int_0^\beta d\tau \sum b_i^\dagger(\partial_\tau - u)b_i + \frac{U}{2}b_i^\dagger b_i^\dagger b_i b_i}$. Expand it to lowest order in powers of hopping, we have

$$\left\langle \exp[-\int d\tau \sum_{i,j}(b_i^\dagger\psi_j + \psi_i^* b_j)]\right\rangle_{S_{loc}} = 1 + \psi_i^* \left\langle \hat{T} b_i^\dagger(\tau) b_i(0)\right\rangle \psi_i.$$

Recall that imaginary time Green's function equals to $-\left\langle \hat{T} b_i^\dagger(\tau) b_i(0)\right\rangle$. Converting it to the frequency space by using Matsubara frequency $\omega_n = 2\pi n/\beta$, It becomes $G(i\omega_n) = \frac{n_0+1}{i\omega_n+\mu-Un_0} - \frac{n_0}{i\omega_n+\mu-U(n_0-1)}$.

Re-exponentiate the resulting series in powers of ψ, and expand the terms in spatial and temporal gradients of ψ, we have Landau free energy as[6]

$$L = K_1\psi\partial_\tau\psi + K_2|\partial_\tau\psi|^2 + K_3|\nabla\psi|^2 + r|\psi|^2 + \frac{u}{2}|\psi|^4, \tag{4}$$

where $r = \frac{1}{ZJ} + G(0)$ and $K_1 = \partial r/\partial\mu$. The phase transition happens when r changes sign, this corresponds to

$$\frac{1}{ZJ} - [\frac{n_{MI}+1}{Un_{MI}(\mu/U) - \mu} + \frac{n_{MI}(\mu/U)}{\mu - U(n_{MI}(\mu/U) - 1)}] = 0. \tag{5}$$

where n_{MI} is the occupation number of each site at Mott insulator state. The corresponding zero-temperature phase diagram is shown in Fig.4(a).

3.2 Universality Class of Quantum Phase Transition

In Fig.4(a), there are two kinds of quantum phase transition, each belongs to its own universality class. In the state of Mott insulator, the density is always pinned at some integer number. As it undergoes a phase transition to the superfluid state, there are two possibilities: either (1) the density remains the same, or (2) the transition is accompanied by a change in density.

- ***Constant density.*** It happens as shown by the blue dash line in Fig.4(a), across the Mott lobe's tip. At fixed chemical potential, sufficiently large hopping term will allow particles to overcome the on-site repulsion and move around the whole system, thereby the system transforms into a superfluid state. In this case, the parabolic shape of phase boundary suggests that $\partial r/\partial\mu = 0$ at the critical point, so $K_1 = 0$ in Eqn.(4), and it is just a $d = 2 + 1$ XY model. (To see this, we could substitute $\hat{b_i} = |\sqrt{\rho_0}|e^{i\phi}$ into H_{BH}, and expand to quadratic order in ϕ, then H_{BH} will go back to H_{XY}).

- ***Various density***. Starting from any point in the $\mu - J$ plane, as the chemical potential increases at fixed J, one will eventually reach a point where the kinetic energy gained by adding another particle into the system will balance the cost of potential energy. This extra particle can hop around the whole lattice without energy cost, producing a superfluid state. In this case, $K_1 \neq 0$, so $|\partial_\tau\psi|^2$ becomes irrelevant.

Since the static and dynamic quantities are inextricably linked in the vicinity of zero temperature, besides the conventional correlation length ξ, characteristic time Ω is necessary for the scaling description; since we expect Ω diverges at the transition point, we have $\Omega \sim \xi^z$, which defines the dynamical exponent z.

Define the reduced chemical potential as $\delta = \frac{\mu-\mu_c}{J}$. The finite size scaling form for the free energy density is

$$f(\delta, \beta^{-1}, L^{-1}) = l^{-(d+z)} f(\delta l^{1/\nu}, \beta^{-1} l^z, l L^{-1}) = \delta^{\nu(d+z)} f(\beta^{-1}\delta^{-\nu z}, L^{-1}\delta^{-\nu}) \tag{6}$$

Here we will figure out the critical exponents through a simple argument. The mean field theory predicts that $\nu = \frac{1}{2}$, but how about dynamic exponent z? First, consider the constant density transition occurred at the Mott lobe's tip. Since $K_1 = 0$ in this case, Landau free energy is isotropic for space and time, We expect that $z = 1$. The situation changes for the various density case. The terms for spatial and temporal variance are $\psi\partial_\tau\psi \sim \frac{\psi^2}{\tau}$ and $(\nabla\psi)^2 \sim \frac{\psi^2}{r^2}$, respectively. Naive power counting implies that $\Omega \sim \xi^2$, i.e, $z = 2$. More strict argument can be found in Ref.[6].

However, the experimental observable is the superfluid density, we need to investigate its behavior near the critical point, rather than the free energy. The density at the superfluid side is $\rho_s = -\frac{\partial f}{\partial \mu} \sim \delta^{\nu(d+z)-1} F(\beta^{-1}\delta^{-\nu z}, L^{-1}\delta^{-\nu})$; it could also be written as

$$\rho_s \sim \delta^{\nu(d+z)-1}(\beta^{-1}\delta^{-\nu z})^{\frac{\nu(d+z)-1}{\nu z}} F(\beta^{-1}\delta^{-\nu z}, L^{-1}\delta^{-\nu}) \sim \beta^{-\frac{\nu(d+z)-1}{\nu z}} \tilde{F}(\delta^{\nu z}\beta, L\delta) \tag{7}$$

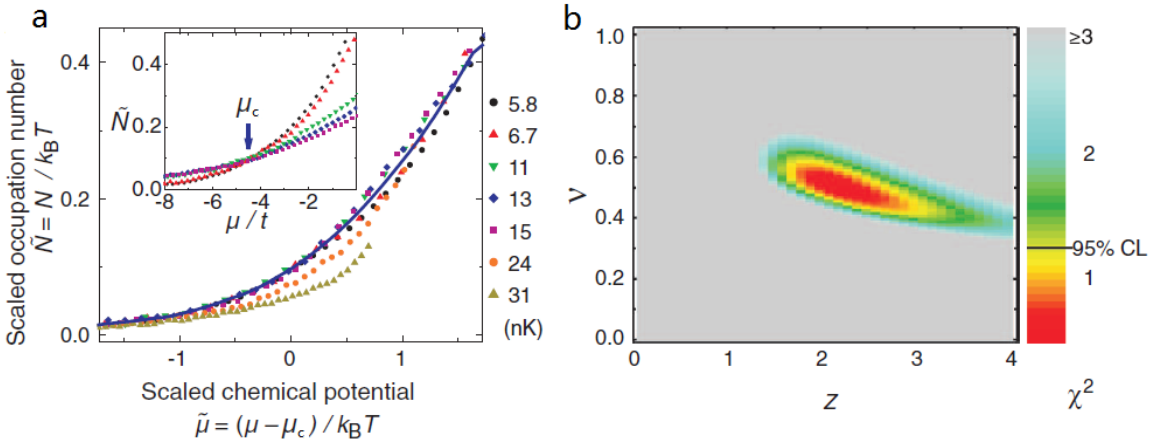

Figure 5: (a) Collapsed occupation number as a function of the scaled chemical potential. The blue solid line is the average curve for the lowest four temperatures. Inset shows the determination of critical chemical potential from curves with different temperatures. (b) Determination of the correlation length exponent ν and dynamical exponent z, based on $u_c = 4.5J$. The color represents the reduced chi-squared (χ^2), indicating how well the data can collapse into a single curve. (From Ref[8])

3.3 Observation of Quantum Criticality with Ultracold Atoms in Optical Lattice

When it comes to the issue of realistic experiment, the finite temperature effect deserves more attention. Suppose that we reduce the chemical potential at fixed J (along the red curve in Fig.4(a)), from Eqn.(6), we except a crossover region where $\delta^{\nu z} \sim T$, instead of a critical point A. Fig.4(b) illustrates the finite-temperature phase diagram and Fig.4(c) is the corresponding experimental result.

The experimental measurement becomes promising, because the superfluid density can be measured directly from in situ density distribution; the chemical potential μ and temperature T are obtained by fitting momentum distribution based on mean-field model. The only unknown parameter is the critical chemical potential μ_c. Eqn.(6) implies that if $\mu = \mu_c$, $\delta = 0$, the free energy density is independent of T. Hence, if we plot $\rho_s(\mu, T)$ versus u for different T, all the curves should intersect at u_c (as shown in the inset of Fig.5(a)).

The experiment[8] is based on ^{133}Cs in two-dimensional optical lattice. The temperature is controlled within the range of 5.8 to 31nK. From the crossing point in the inset of Fig.5(a), the critical chemical potential μ_c is determined as $\mu_c = -4.5(6)t$, which agrees with the theoretical prediction $\mu_0 = -4t$ derived from Eqn.(5).

On the basis of the expected exponents $z = 2$ and $\nu = \frac{1}{2}$, Eqn.(7) becomes $\rho_s/k_BT \sim \tilde{F}[(\mu - \mu_c)/k_BT]$ for constant J. Fig.5(a) shows the scaled occupation number as a function of scaled chemical potential. Below 15nK, they collapse into a single curve, demonstrating the emergence of quantum criticality. Deviations become obvious for higher temperature. Next, to examine the critical exponents, various values of z and ν are taken to check how well the data can collapse to a single curve. The evaluation shows that the best-fit exponents are determined as $z = 2.2^{+1.0}_{-0.5}$ and $\nu = 0.52^{+0.09}_{-0.10}$(as shown in Fig.5(b)). They agree with our

previous argument: $z = 2$ and $\nu = \frac{1}{2}$.

4 Summary and Discussion

As a summary, in this paper, we first discussed BKT transition in terms of XY model, and the RG analysis provides a deep view of this phenomena. Experimental results provide not only a microscopic detection of BKT transition, but the critical exponents expected by theoretical prediction. In the second part, we introduce the Bose-Hubbard model, which can be emulated by optical lattice. A simple theoretical argument gives the scaling form and critical exponents; and such quantum critical behavior has been observed experimentally.

For achieving further progress, one of the most challenging issues for cold gases system is the difficulty to determine temperature. The cold atomic system is isolated from external ensemble, so the lack of extrinsic thermometer preventing the conventional temperature measurement. Nowadays, the information about temperature is obtained from intrinsic properties of cold gases, e.g. by fitting the momentum distribution to a given theoretical model, though the validity of the theoretical calculation deserves further investigation. This difficulty becomes more obvious in strongly correlated problems. The lack of general theory in this region prevents AMO researchers connecting what they observe to the quantities in conventional condensed matter system. Therefore, finding a convincing thermometer may be the next important task for this area.

References

[1] The theoretical approach to XY model is based on Quantum Field Theory in Condensed Matter Physics, Chapter 3.3, N. Nagaosa. Springer(1999)

[2] A. Alexander and B. Simons, Condensed Matter Field Theory, Chapter 8.6. Cambridge Univ Press(2006)

[3] Z. Hadzibabic, P. Kruger, M. Cheneau, B. Battelier and J. Dalibard, Nature 441, 1118 (2006).

[4] Polkovnikov, A., Altman, E. & Demler, E. Proc. Natl Acad. Sci. USA 103, 6125(2006).

[5] W.S. Bakr, A. Peng, M.E. Tai, R. Ma, J. Simon, J.I. Gillen, S. Folling, L. Pollet and M. Greiner, Science 329, 547(2010).

[6] M.P.A. Fisher, P.B. Weichman, G.Grinstein and D.S. Fisher, Phy. Rev. B 40, 546(1989).

[7] X. Zhang, C.L. Hung, S.K. Tung, N. Gemelke and C. Chin, New J. Phys. 13, 045011(2011)

[8] X. Zhang, C.L. Hung, S.K. Tung and C. Chin, Science 335, 1070(2012)